HAL
open science

Experimental study of the transport properties of rough self-affine fractures

Franck Plouraboué, Pascal Kurowski, Jean-Marc Boffa, Jean-Pierre Hulin, Stéphane Roux

To cite this version:

Franck Plouraboué, Pascal Kurowski, Jean-Marc Boffa, Jean-Pierre Hulin, Stéphane Roux. Experimental study of the transport properties of rough self-affine fractures. Journal of Contaminant Hydrology, 2000, 46 (3-4), pp.295-318. 10.1016/S0169-7722(00)00134-0 . hal-03604955

HAL Id: hal-03604955

https://hal.science/hal-03604955v1

Submitted on 10 Mar 2022

HAL is a multi-disciplinary open access archive for the deposit and dissemination of scientific research documents, whether they are published or not. The documents may come from teaching and research institutions in France or abroad, or from public or private research centers.

L'archive ouverte pluridisciplinaire **HAL**, est destinée au dépôt et à la diffusion de documents scientifiques de niveau recherche, publiés ou non, émanant des établissements d'enseignement et de recherche français ou étrangers, des laboratoires publics ou privés.

Experimental study of the transport properties of rough self-affine fractures

Franck Plouraboué [a,b,c], Pascal Kurowski [b], Jean-Marc Boffa [c], Jean-Pierre Hulin [c,*], Stéphane Roux [d]

[a] *Institut de Mécanique des Fluides, UMR CNRS no. 5502, Allée du Pr C. Soula, 31400 Toulouse, France*
[b] *Laboratoire de Physique et de Mécanique des Milieux Hétérogènes, UMR CNRS no. 6536, Ecole Supérieure de Physique et Chimie Industrielles de Paris, 10, rue Vauquelin, 75231 Paris Cedex 05, France*
[c] *Laboratoire Fluides, Automatique et Systèmes Thermiques, UMR CNRS no. 7608, Bâtiment 502, Université Paris-Sud, 91405 Orsay, France*
[d] *Surface du verre et Interfaces, UMR CNRS / Saint-Gobain no. 125, 39 Quai Lucien Lefranc, 93303 Aubervilliers Cedex, France*

Abstract

An experimental study of the transport properties of fluid-saturated joints composed of two complementary rough fracture surfaces, translated with respect to each other and brought in contact, is reported. Quantitative roughness measurements on different fractured granite samples show that the surfaces have a self-affine geometry from which the dependence of the mean aperture on the relative displacement of fracture surfaces kept in contact can be predicted. Variations of the hydraulic and electrical conductances of the joint are measured as functions of its mean aperture. A simple parallel plane model accounts for the global trend of the measurements, but significant deviations are observed when a relative lateral displacement of the surfaces is introduced. A theoretical analysis of their origin shows that they are due both to the randomness of the aperture field and to a nonzero local slope of the surface near the injection hole; the corresponding conductivity fluctuation amplitudes have power law and linear variations with the lateral displacement, and are enhanced by the radial injection geometry.

Keywords: Fracture; Self-affine; Roughness; Flow; Permeability; Conductivity

[*] Corresponding author. Fax: +33-1-69158060.
E-mail address: hulin@ariane.fast.u-psud.fr (J.-P. Hulin).

1. Introduction

1.1. Interest and geometrical characteristics of natural fractures

Fractures are very common features of earth's upper crust and range from large-scale faults to microcracks. Fluid flow through fractures is a very important mechanism in porous media with small intrinsic permeability; it greatly influences transport processes both in natural crystalline and tight sedimentary rocks (granite, basalt, low-permeability sandstone, etc.) and in artificial structures (concrete, cement). In addition, fluid transport in fractured rocks is relevant to a number of geophysical applications, such as hazardous waste storage, hydrogeology, and geothermal and petroleum engineering (Evans et al., 1992; Petitjean and Couet, 1994). Understanding transport properties of natural fractures, particularly their relation to variations of the local aperture $a(\vec{x})$ (cf. Fig. 1), is, thus, crucial for numerous applications.

The objective of the present work is to experimentally analyze the dependence of these transport properties on fracture roughness. An important step in modelling the topography of fracture surfaces has been the observation that these surfaces are well-described as self-affine structures (Bouchaud et al., 1993) in various natural and man-made materials, such as granite (Brown, 1988), marble (Poon et al., 1992), sandstone (Plourabouré et al., 1996) and concrete (Schmittbuhl et al., 1995), as well as in natural faults (Power et al., 1987). Such surfaces satisfy a scale invariance (Feder, 1988; Falconer, 1990), and are statistically unchanged under the transformation

$$\begin{cases} x \to \lambda_{\parallel} x \\ y \to \lambda_{\parallel} y \\ z \to \lambda_{\perp} z \end{cases} \tag{1}$$

in which z is perpendicular to the mean fracture plane, and x and y are parallel to it. The dilation ratios $\lambda_{\parallel}$ and $\lambda_{\perp}$ are related through $\lambda_{\perp} = \lambda_{\parallel}^{\zeta}$, where ζ is called the roughness exponent (or Hurst exponent) (Feder, 1988). Experimental ζ values are close to 0.8 ± 0.05 for many materials and fracture mechanisms (lower values of the exponent have, however, been obtained at small scales or for materials fractured at a finite fraction of the acoustic Rayleigh wave speed, or yet, for some loosely consolidated granular materials). These geometrical properties imply the existence of long-range (infinite) correlations in the topography of the fracture surface; these result in scale effects that must be considered when extrapolating laboratory-scale measurements to field applications. The question, then, is: how can scaling laws relating length scales parallel and perpendicular to the fracture plane be translated into scaling laws for transport properties, such as the hydraulic and electrical conductances of fractures (Roux et al., 1993)? For such applications, it is essential to take into account the correlation between the two faces of the crack (Brown, 1986), and simple phenomenological models have been developed to introduce such geometrical correlations (Brown, 1995; Mourzenko et al., 1996).

The present paper considers a crack bounded by two complementary self-affine surfaces (the two halves of the same fracture block) translated with respect to each other

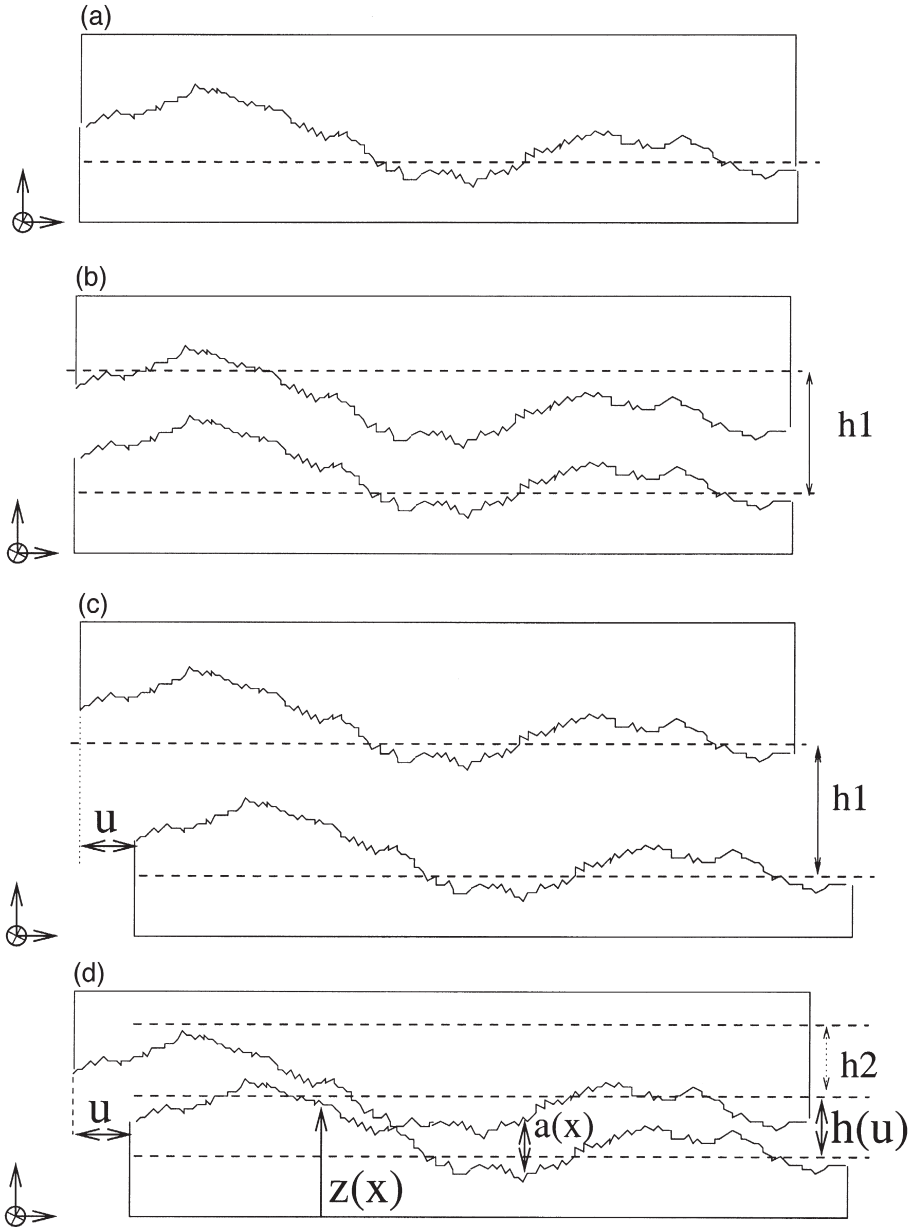

Fig. 1. Schematic representation of the experimental rough crack. Rough faces are complementary and in perfect contact at the begining of the experiment (a). Then, the lower block is moved vertically (b) by a distance h_1, laterally by a distance u (c), and back vertically to contact by a distance h_2 (d). The vertical distance between each block is thus $h(u) = h_1 - h_2$, which is also the mean aperture. The fracture height $z(x)$ is represented as well as the local aperture $a(x)$.

and brought into contact (Fig. 1d), or were left separated (Fig. 1c). A model describing the local thickness distribution in such a configuration had been previously suggested (Plouraboué et al., 1995). Hereafter, the in-plane component of the relative displacement is referred to as the "shift" u. When both surfaces are in contact, the normal component h is a function of u, i.e. $h \equiv h(u)$ for a given direction of the displacement. The local aperture $a(x,y)$ is then related to $h(u)$ and to the height profile $z(x,y)$ of the fracture surface by

$$a(x,y) = z(x+u,y) - z(x,y) + h(u). \tag{2}$$

This assumes that the two surfaces are perfectly mated for a zero lateral shift ($u = 0$), which amounts to neglect the effect of surface wear. The results from Eq. (2) show that $h(u)$ coincides with the spatial average of the aperture: $h(u) = \langle a(x,y) \rangle$. In a previous work (Plouraboué et al., 1995), a statistical analysis of $h(u)$ for a self-affine surface was suggested. It was demonstrated theoretically and experimentally (Plouraboué et al., 1995) that $h(u)$ also depends on the length L of the crack and varies as

$$h(u) = u^{\zeta} K \sqrt{1 + K' \log(L/u)} \tag{3}$$

where u/L is the relative amplitude of the shift of the joint, ζ is the roughness exponent of the crack surface, and K and K' are two constants. This result has been verified both experimentally on a fractured granite block and through numerical simulations on computer-generated self-affine surfaces (Plouraboué et al., 1995). This scaling law is important for extrapolating experimental laboratory results to the field scale.

1.2. Models of flow in fractures

Many authors have studied the influence of variations of the local fracture aperture on fluid transport properties experimentally (Witherspoon et al., 1980; Brown et al., 1989), theoretically (Ge, 1997) and numerically (Tsang et al., 1988; Rasmuson and Neretnieks, 1982; Brown, 1987; Gutfraind and Hansen, 1995; Mourzenko et al., 1995; Zimmerman et al., 1991). A lowest-order approach to model flow properties is to represent the fracture as two parallel surfaces separated by a distance h. Then, the fluid flow rate across a section of the fracture is proportional to the applied hydraulic pressure gradient and to the cube of the separation distance h. Such a simple law is, however, of limited use (Evans et al., 1992), particularly when h is of the order of magnitude of the surface roughness.

•In the laminar flow regime, variations of the local spacing between fracture surfaces as well as the tortuosity of the flow paths may influence the permeability (Ge, 1997). The simplest way to take these effects into account is to use the Reynolds (or lubrication) approximation (Pinkus and Sternlicht, 1961). In this case, one considers only the in-plane (x,y) component of the velocity field (the vertical component is ignored), whose distribution is approximated by a local parabolic Poiseuille profile. The square $a(x,y)^2$ of the local aperture represents a local Darcy permeability, and the macroscopic permeability depends on the distribution of the local apertures. The local velocity $\vec{V}_m$ should then be related to the viscosity μ and to the pressure gradient $\vec{\nabla} P$ by

$$\vec{V}_m = -\frac{a^2(x)}{12\mu} \vec{\nabla} P. \tag{4}$$

The Reynolds approximation is valid when the aperture gradient (and thus, the local slope of the surface) is much smaller than unity, i.e. $|\nabla a| \ll 1$. For self-affine cracks, the averaged slope estimated at a scale l varies as $l^{\zeta-1} \simeq l^{-0.2}$, and therefore increases at smaller length scales. However, experimental profile measurements on all tested samples have shown that local slopes are small above a scale l of 50 μm. Hence, the Reynolds approximation should be valid for fractures with mean apertures above a few tens of microns. Experimental data will be analyzed in Section 5 in the context of the Reynolds approximation.

•In the inertial regime, even with small local slopes, the Reynolds approximation fails because nonlinear terms of Navier–Stokes equation are not negligible anymore (Gutfraind and Hansen, 1995; Brown, 1995). Such effects are not considered in the present work since all measurements are carried out in the range of linear variation of the total flux with the applied pressure.

Although a large number of theoretical and numerical studies have been devoted to the transport properties of rough cracks, few have experimentally addressed the effect of roughness in natural fractured rocks (Witherspoon et al., 1980; Brown et al., 1989; Brown, 1985). The present work first confirms and experimentally extends previous geometrical results obtained on self-affine rough fractures to the different samples for which transport properties will be analyzed. After describing the experimental set-up and the characterization of fracture surface roughness, measurements of the influence of the sample size on the geometrical aperture of different granite joints are discussed. More precisely, fluctuations (standard deviation σ_h) of the mean aperture $h(u)$ for two blocks in contact are studied for a varying orientation of a relative displacement $\vec{u}$ of constant amplitude in the mean plane of the fracture. This experimental study is complemented by numerical simulations of geometrical properties of the joint. Then, the transport properties of rough joints saturated with a fluid are investigated experimentally. Flow measurements are realised in the domain of linear variation of the pressure gradient with the flux. The variation of both electrical and hydraulic conductances is analyzed as a function of the normal, $h(u)$, and lateral, u, relative displacements between joint faces. Large fluctuations of the electrical conductance, only partly correlated to aperture variations, are observed and studied theoretically.

2. Experimental procedure

2.1. Rock samples

Experiments were performed on fractured granite and basalt blocks of initial size $25 \times 25 \times 15$ cm^3. Two parallel notches were first carved in the middle of two opposite faces, and a mode I crack (Scholz, 1990) was propagated from one notch to the other. Two types of rocks have been used to test the sensitivity of the results to the nature of the material. The first two blocks are made of grey granite with coarse millimetric-size heterogeneities (sample nos. 1 and 3, originating from Brittany, France). The basalt block is black and finely grained (sample no. 2, originating from Africa). Both materials

are very strongly consolidated so that fractures propagate through the heterogeneities. In both cases, the fracture roughness displays a very broad range of characteristic length scales (from 100 μm to a few cm), as expected for a self-affine surface.

2.2. Profilometry measurements

Fracture surfaces are characterized using a mechanical profilometer of 2 μm resolution perpendicular to the mean fracture plane and 25 μm parallel to it. Height profiles are measured on the fracture surface along parallel straight segments, and the repeatabil-

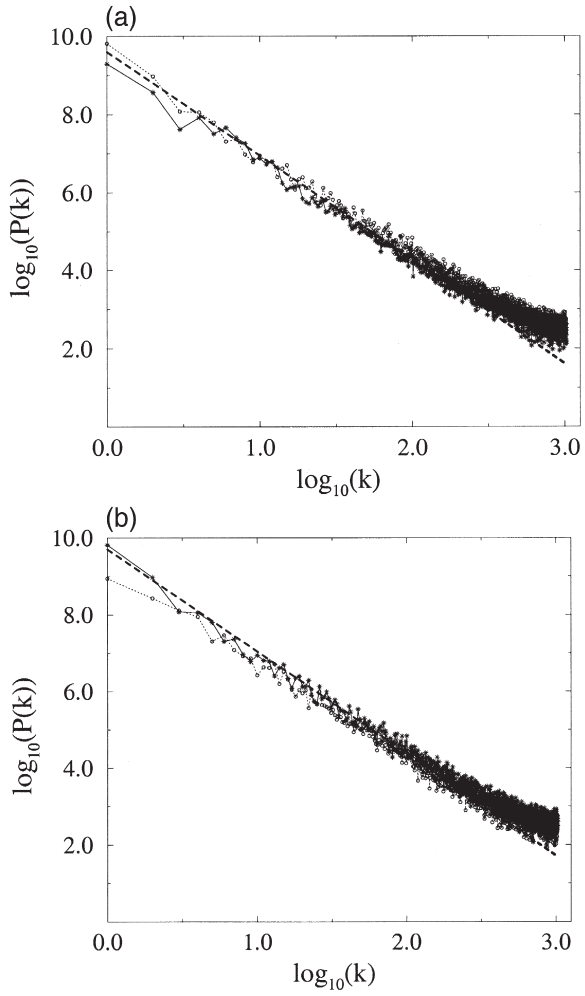

Fig. 2. Mean Fourier power spectra of height profiles measured on the surface of fractured granite blocks. Dashed lines correspond to the slope of the estimated rough exponent ζ of Table 1. (a) Superposition of two power spectra obtained from measurements carried out on two perpendicular directions on sample no. 2. (b) Superposition of two power spectra obtained from measurements carried out on samples nos. 1 and 2.

ity on the height values is of order 10 μm. The typical length of the segments is 100 mm and the distance between neighboring profiles is 400 μm. One of the halves of the fractured block is put horizontally on the sensing assembly with the fracture surface oriented upward. The local height is measured by lowering a fine-tipped sensor onto the surface and recording the position at which contact is detected; the cycle is then repeated for all points over the profile with a horizontal spacing of 50 μm. The roughness exponent ζ can be determined, for instance, by computing the Fourier spectrum $P(k)$ of the height $z(x)$ of the surface along a profile. For self-affine profiles, $P(k)$ can be shown to obey (Brown, 1988; Poon et al., 1992; Plourabouré et al., 1996; Schmittbuhl et al., 1995)

$$P(k) = |\tilde{z}(k)|^2 \propto k^{-1-2\zeta}. \tag{5}$$

Fig. 2a displays two average Fourier power spectra obtained from block no. 2 using profiles measured in two perpendicular directions. Each spectrum corresponds to the average of ten 2048-point parallel profiles. The near coincidence of the spectra suggests an isotropy of the self-affine properties of the surface. Fig. 2b displays superimposed average spectra corresponding to a granite and a basalt sample (block nos. 1 and 2). Roughness exponents ζ are estimated from the slopes of Fig. 2a and b using Eq. (5). Both exponents are very close to the 0.8 value reported by other authors on granite and other types of materials. The standard deviation $\sigma_z(L)$ of the height of the sample surface of a profile segment of length L is finally expected to scale according to

$$\sigma_z(L) = ML^{\zeta} \tag{6}$$

The parameter M characterizes the amplitude of the roughness and is lower for the finer grained basalt sample than for the coarser granite ones. Values obtained by computing $\sigma_z(L)$ over segments of length $L = 10$ cm are listed in Table 1.

2.3. Transport properties measurement set-up

Transport properties are analyzed on a second set-up allowing both hydraulic permeability and electrical conductance measurements (Fig. 3). The lower block can be moved vertically (with an amplitude of 12 mm) and in both horizontal directions with an amplitude of ± 25 mm by micrometric translation devices. The upper block is allowed to move only upwards from a rest position adjusted initially with both halves of the fractured block in contact. Sideway motions are blocked by ballpoint devices pressed against the edges. Downward motion from the initial position is prevented by adjusting the propping system with the two blocks in contact. Displacements of both blocks in all

Table 1

Sample number	Roughness exponent ζ	σ_z (cm)	Roughness magnitude M
1	0.83 ± 0.05	1.33	0.19 $cm^{0.17}$
2	0.79 ± 0.06	0.94	0.15 $cm^{0.21}$
3	0.80 ± 0.06	1.39	0.22 $cm^{0.2}$

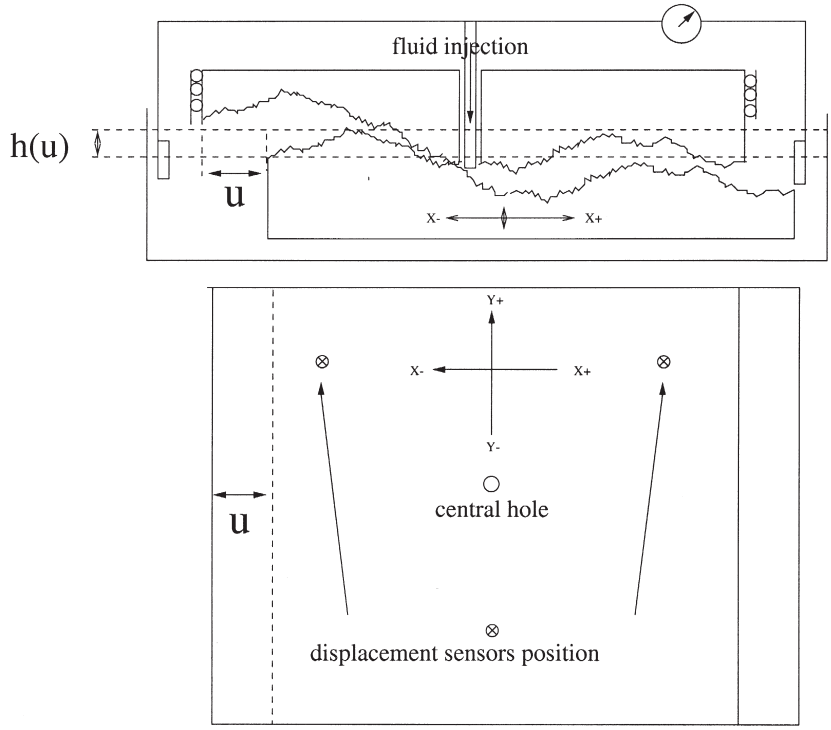

Fig. 3. Experimental set-up for measuring transport properties on an artificial fracture made of two fractured granite or basalt blocks translated and brought back to contact along the fracture surface (horizontal and top view).

directions are permanently monitored with a resolution of ± 5 μm by mechanical sensors. After each set of measurements, one verifies that the blocks come back in contact over the whole fracture surface when the lower block is brought back to its initial position. This is checked by raising the lower block after it has touched the upper one and by verifying that upward displacements measured by three sensors at different points on the upper block are identical. In situations where the blocks have a relative horizontal displacement, they are considered to be in contact when any of the sensors located on the upper block detects an upward motion larger than 10 μm.

The sample is then plunged inside a parallelepipedic basin filled with water so that the liquid surface is always above the uppermost point of the fracture. In this way, it always remains saturated with water once trapped air has been sucked away. For a given relative position of the blocks, the hydraulic conductance is measured by injecting fluid at a constant flow rate through a vertical 5-mm borehole drilled at the center of the upperblock. Injected fluid flows out on the sides. The injected flow field is only approximated to be radial because of the square outer shape of the blocks. This does not have much influence on the transport properties since most of the pressure drop is localized near the injection. The effective hydraulic conductance of the fracture joint is

determined by measuring the pressure difference ΔP between the injection point and the rim of the fracture at five different flow rates spanning one order of magnitude. Finally, a linear regression is performed on each data set. A 40%:60% glycerol–water mixture is used as the flowing fluid in order to increase the measured pressure and reduce the Reynolds number (resulting in more linear pressure vs. flow rate relations). ΔP is measured through a sensing tube opening close to the fracture surface in the injection borehole. This allows the elimination of the effect of the pressure drops in the injection circuits. The other end of the tube is connected to one of the ports of a Validyne DP15 differential pressure sensor. The other port is connected to another measurement point located at the rim of the fracture. The range of the sensor is $\pm 10^4$ Pa and its precision is 0.1%. Flow rates range between 4×10^{-8} and 2.5×10^{-6} m^3/s, and can be adjusted by steps of 2×10^{-9} m^3/s. The electrical admittance is determined with an HP 4192A computer-controlled bridge after saturating the fracture with a 1 g/l $NaNO_3$–water solution. The measurement frequency is 20 kHz, which minimizes the reactive component of the impedance and allows a precision of 0.01% to be obtained. Measurements are performed between a cylindrical movable electrode inserted into the injection borehole and a set of brass plates located in the fluid bath outside the blocks. The center electrode is lowered down to the lower block surface in order to extend vertically across the full fracture aperture.

3. Geometrical measurements

The geometrical characterization of the samples by profilometry has been complemented by measuring the vertical spacing $h(u = |\vec{u}|)$ between the two blocks kept in contact as a function of the horizontal displacement $\vec{u}$ (Plourabouré et al., 1995). Experimental results obtained with sample nos. 2 and 3 for four different orientations of $\vec{u}$ at 90° intervals are shown in Fig. 4a–b. The four curves coincide quite well up to relative displacements $u/L > 0.05$ for which $\pm 30\%$ deviations may be observed. Let us now investigate in more details these variations of $h(\vec{u})$ as a function of the orientation of the displacement.

Fig. 5 displays for sample no. 2 the variation of $h(\vec{u})$ as a function of the angle θ of the vector $\vec{u}$ with respect to a reference axis. The data correspond to three displacement amplitudes $|u|$ equal to 1, 3 and 10 mm, and to 32 different θ values. The corresponding values of the standard deviation $\sigma_h(u)$ of $h(u)$ from its mean $\langle h(u) \rangle_\theta$ are shown in Table 2 for sample nos. 2 and 3. The relative deviation $\sigma_h(u)/h(u)$ clearly increases with the lateral displacement $|u|$. This variation is a relevant additional information on the structure of the fracture joint. A numerical investigation of this problem is reported in Section 5.1.

Finally, the scaling law of Eq. (3) is checked by plotting the ratio $h^2(u)/u^{2\zeta}$ as a function of $\log(u/L)$. The values of ζ used are those obtained from mechanical profilometry measurements (Table 1). In Fig. 6a–b, $h(u)$ is the average of the four curves displayed in Fig. 4a–b. Data points (symbol *) corresponding to an average over all θ values in Fig. 5 have also been plotted in Fig. 6b, and coincide well with the

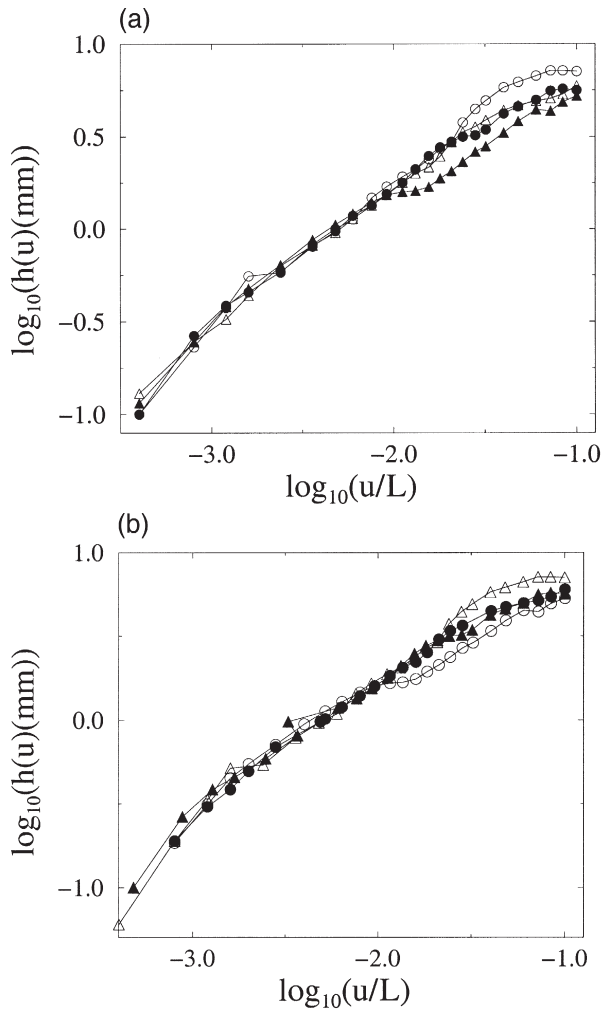

Fig. 4. Mean aperture $h(u)$ (in mm) vs. horizontal relative displacement u/L ($L = 25$ cm) for the two parts of fractured granite and basalt blocks displaced relative to each other, with respect to their initial adjustment position while remaining in contact at least on one point. The four symbols (open and shaded triangles and circles) correspond to orientations of the displacement in four different directions noted $x+$, $x-$, $y+$ and $y-$ in Fig. 3. (a) Sample no. 3. (b) Sample no. 2.

overall variation. This suggests that averages performed over four different orientations of the displacement $\vec{u}$ are sufficiently representative. As expected, $h^2(u)/u^{2\zeta}$ decreases linearly with $\log(u/L)$, except at very small displacements. One possible origin of the discrepancy is the fact that, due to damage associated with the fracturing process at small scales, the two halves of a fractured block do not coincide perfectly when put back together. Introducing a small constant shift of roughly 100 μm on the aperture values (Plourabouè et al., 1995) improves the agreement with the theoretical predictions down

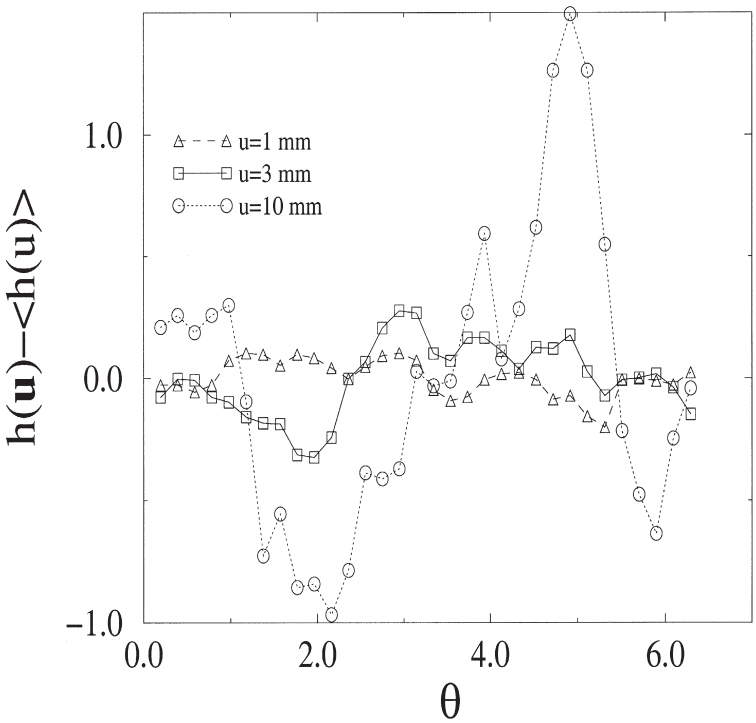

Fig. 5. Spatial mean aperture $h(u,\theta)-\langle h(u)\rangle_\theta$, as a function of the orientation ($\vec{u}=u\vec{e}(\theta)$ with $\theta\in[0,2\pi]$) of the horizontal displacement for constant displacement moduli equal to $u=1$, 3 and 10 mm. Respective values of aperture $\langle h(u)\rangle$ are: 0.794, 1.78, 4.47 mm.

to the smallest scales. This vertical shift represents a residual aperture, and will also appear in transport measurements discussed in Section 4. Small secondary fractures branching away from the surface at a small angle have been observed and may account, in part, for the residual aperture. Another possible origin is the removal of some asperities during fracture propagation. It is also worth noting that the plots of Fig. 6a–b are very sensitive to the choice of ζ, and that the variation of $h^2(u)/u^{2\zeta}$ is no longer linear if ζ varies by 15% or so. Values of the coefficients K and K' in Eq. (3) deduced

Table 2

Sample number	Relative shift u (mm)	Mean aperture $\langle h(u)\rangle$ (mm)	Fluctuations of $h\sigma_h(u)$ (mm)	Relative fluctuations $\sigma_h/\langle h\rangle$
2	1	0.72	0.096	0.09
2	3	1.62	0.14	0.109
2	10	4.07	0.64	0.22
3	1	0.92	0.07	0.08
3	3	1.98	0.15	0.075
3	10	4.3	0.61	0.14

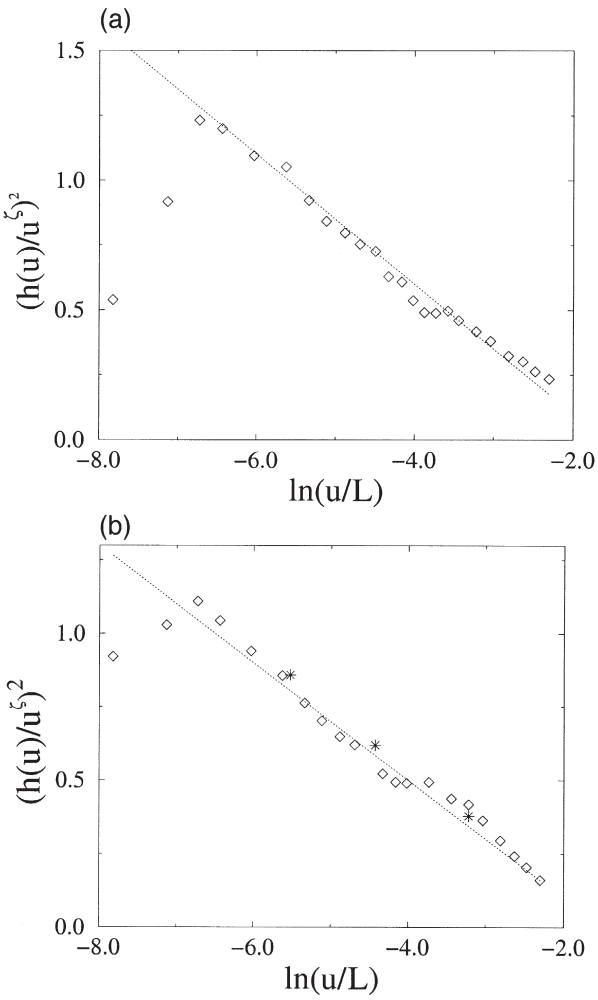

Fig. 6. Variations of the normalized squared mean vertical displacement $h(u)^2/u^{2\zeta}$ as a function of $\ln(u/L)$ for the granite and basalt samples used in the present study. ◇ corresponds to average of $h(u)$ over four different displacement orientations at right angle from each other, * corresponds to average over 32 different orientations of $\vec{u}$ for the three data series of Fig. 4a. (a) Granite sample no. 3. (b) Basalt sample no. 2.

from the data of Fig. 6a–b are listed in Table 3. K is a useful characterization of the roughness amplitude. Experiments on two very different types of samples reported in this section therefore confirm previous experimental results and theoretical predictions

Table 3

Sample number	K (mm$^{0.2}$)	K
2	0.19	9
3	0.18	3.6

(Plourabouré et al., 1995), such as Eq. (3) relating the horizontal and normal displacements of two complementary self-affine surfaces in contact. Significant relative variations of the aperture as a function of the orientation of the displacement vector $\vec{u}$ have, however, been observed, particularly at large amplitudes. In the next part, the dependence of transport parameters on the amplitude and orientation of $\vec{u}$ is investigated on the same set of samples.

4. Transport measurements

4.1. Electrical conductance measurements

The measurement technique is calibrated by moving vertically apart the two halves of the fractured block from the position of optimal contact; the blocks are kept parallel with a zero relative horizontal shift so that their local spacing is constant over the fracture surface. Then, the effective electrical admittance should be similar to that of two parallel planes with a distance equal to the relative normal displacement h. One may only expect a second order effect due to the roughness that increases the effective distance between the center electrode and the outside ones. The dotted lines in Fig. 7a–b (symbols *) represent the variation of the electrical admittance with the vertical relative displacement h; this variation is nearly linear and its slope can be estimated by modelling the fracture as a set of two parallel disks of radius R and separation h with an inside electrode of radius r_0. The corresponding electrical admittance $A(h)$ is

$$A(h) = \sigma_0 \frac{2\pi h}{\log(R/r_0)} = \sigma_0 K_{\mathrm{el}} \tag{7}$$

where σ_0 is the electrical conductivity of the fluid and K_{el} is a geometrical factor which, for simplicity, will be referred to in the following sections as the electrical conductance. Actually, the complex admittance also includes reactive components of various origins (double layer capacitance on electrodes, for example). The measurement frequency is chosen so that the capacitive component only represents a small fraction (0.1%) of the overall admittance and can be neglected. In Eq. (7), the shape of the outer boundary of the domain is approximated by a circle instead of the actual square boundary. However, the conductance only weakly depends on the actual shape of the outer boundary due to the logarithmic dependence on R in Eq. (7). R is, in the following equations, taken to be equal to half the diagonal of the boundary of the granite samples.

Using σ_0 values measured on the bulk solution, one obtains theoretical values for the slope $2\pi\sigma_0/\log(R/r_0)$ of the dotted curves of Fig. 7b, about 5–7% higher than the experimental ones. This small difference may be due to the roughness of the surface, increasing the effective distance between the inner and outer electrode. Extrapolating the experimental linear variation to zero admittance gives a residual aperture estimate of 120 μm, which confirms geometrical measurements (Fig. 7b).

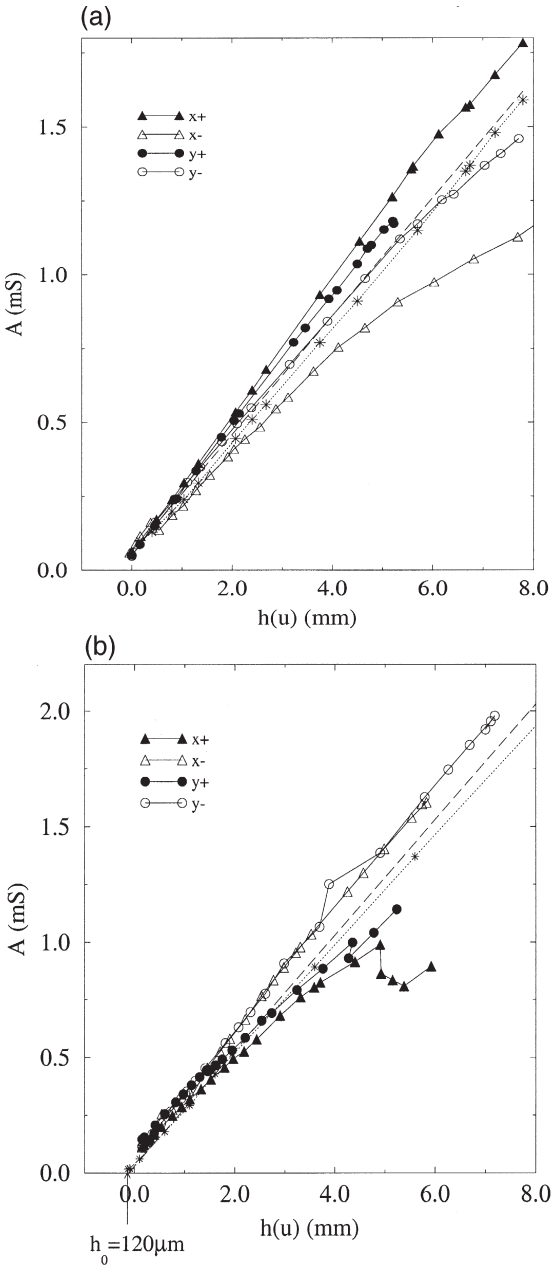

Fig. 7. Variations of the electrical admittance with the relative vertical displacement of two fractured blocks in a radial measurement geometry. Dotted line with * symbols corresponds to a pure vertical displacement (no horizontal shift). Long-dashed line corresponds to theoretical expectation with a parallel plane model. The four symbol sets correspond to different directions of displacement $\vec{u}$. (a) Granite sample no. 3. (b) Basalt sample no. 2.

The admittance is measured after displacing horizontally the two halves of the fractured block, and adjusting the distance h to bring the blocks in contact. Variations of the admittance A with $h(u)$ for four different orientations at right angles of the lateral

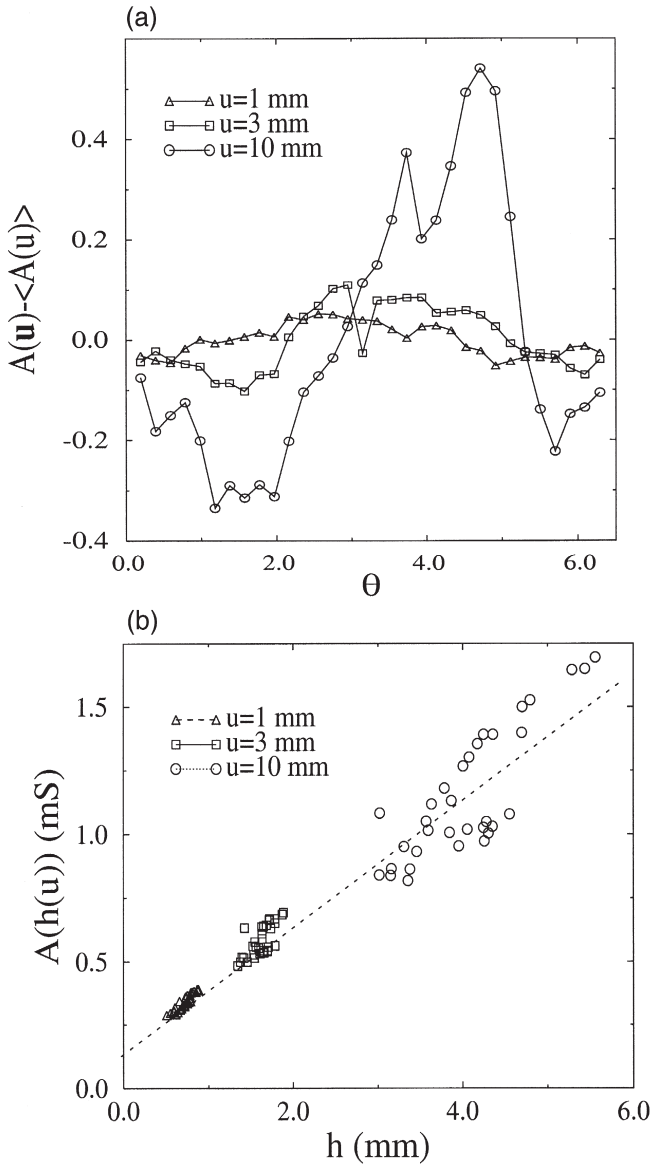

Fig. 8. (a) Fluctuations of the electrical admittance as a function of the orientation of the horizontal displacement for the same horizontal and vertical displacement, as in Fig. 5. (b) Variations of electrical admittance with the spatial mean aperture corresponding to Fig. 5 and (a) data series. Dotted line corresponds to the global linear trend of the data.

displacement are compared in Fig. 7a–b to the previous results obtained for $u = 0$. In all cases, and particularly for $h < 4$ mm, the admittance A roughly increases linearly with $h(u)$; this confirms that the distance h is the adequate scaling variable to describe the electrical conductance, as suggested by the parallel plane model (Eq. (7)). Strong relative deviations from the linear law (up to 20–30%) are, however, observed, particularly for large values of $h(u)$ (and in the $x+$ direction). These variations were investigated in more detail by measuring the electrical admittance A in the same geometrical configuration as in Fig. 5 (constant amplitude $|u|$ and variable orientation of the displacement $\vec{u}$). Fig. 8a displays the variations of A with the angle θ defined as in Fig. 5. The relative amplitude of the variations of A are of orders 14%, 13.5% and 25% for $u = 1$, 3 and 10 mm, respectively. However, a significant fraction of these variations may be due to the fact that $h(u)$ varies significantly with the angle θ (as shown in Fig. 5). In order to separate out this effect, the variations of A corresponding to the data points of Figs. 5 and 8a, and to the three displacement amplitudes $|u| = 1$, 3 and 10 mm, are plotted in Fig. 8b as functions of $h(u)$. As expected, the mean trend of the variation is clearly linear, but significant variations of up to $\pm 15\%$ are still observed, and their amplitude increases markedly with $h(u)$.

In all cases, the normal displacement $h(u)$ is, therefore, the adequate scaling variable controlling the overall variation of the admittance A. The amplitude of the deviations of A from this global linear dependence on $h(u)$ is, however, quite important and tends to increase with h. As will be seen in the next part, similar effects can be observed experimentally for the hydraulic conductance.

4.2. Hydraulic conductance measurements

As for the admittance, hydraulic conductance measurements are first calibrated in a constant aperture geometry (Fig. 1b), with a zero lateral relative shift $|u|$ of the blocks. Practically, the variation of the pressure difference ΔP is measured as a function of the flow rate Q. For a parallel plane geometry and a radial injection, the ratio $Q/\Delta P$ should verify

$$\frac{Q}{\Delta P} = \frac{\pi h^3}{6\eta \log(R/r_0)} = \frac{1}{\eta} K_{\mathrm{hy}}(h) \tag{8}$$

in which η is the dynamic viscosity of the fluid (kept constant for these experiments), r_0 the radius of the central hole for injection, and K_{hy} the hydraulic conductance. The dotted line in Fig. 9 represents, for sample no. 2, the experimental variations of $(Q/\Delta P)^{1/3}$ with the relative displacement h of the blocks normal to the fracture plane (the lateral displacement $|u|$ is zero). A nearly linear variation is observed as expected from Eq. (8). By applying this equation and including the measured fluid viscosity, one obtains for each value of $(Q/\Delta P)^{1/3}$ an effective hydraulic aperture h_{hy} equal to within 8% to the mechanical displacement. As in the case of the admittance, h_{hy} reaches for $h = 0$ a finite limit h_{hy0}; it is the difference $h_{\mathrm{hy}} - h_{\mathrm{hy0}}$ that is actually compared to h.

Hydraulic conductance variations are measured by moving the lower block horizontally over a distance u and putting it in contact again with the upper one (Fig. 1c and d).

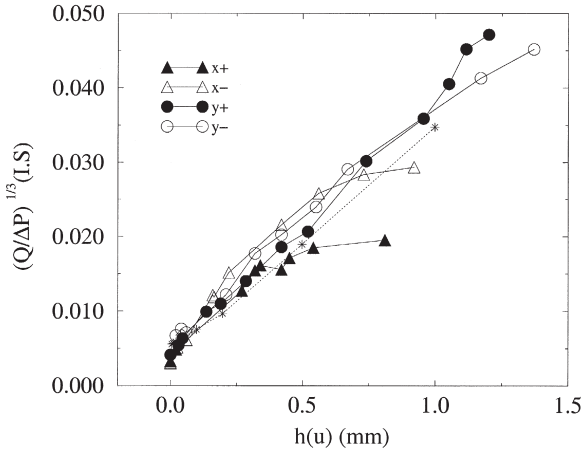

Fig. 9. Variations of $(Q/\Delta P)^{1/3}$ vs. the mean aperture $h(u)$ for the basalt sample no. 2.

As shown in Fig. 9, the overall variation of the hydraulic conductance with the vertical displacement $h(u)$ is roughly cubic for all four orientations of the displacement $\vec{u}$ investigated. Observed relative deviations from this mean law are of order 50%. These variations are not random fluctuations around the mean cubic law, but are systematic deviations which depends on the orientation of the horizontal shift $\vec{u}$. These deviations are expected to be enhanced by the radial geometry; the hydraulic conductance K_{hy} is indeed strongly influenced by the structure of the flow field in the immediate vicinity of the injection hole, where pressure gradients are largest. Let us note that, within Reynolds approximation, K_{hy} is much more sensitive to aperture variations than the electrical conductance, due to its cubic dependence on the local aperture ($K_{\mathrm{hy}} \propto \langle a(\vec{x})^{-3} \rangle^{-1}$).

In this section, it has been shown that the parallel plane model provides a reasonable first-order description of the transport properties of natural fracture joints. Electrical and hydraulic conductance values in the radial geometry display globally linear and cubic variations with the mean aperture. On the other hand, lateral displacements of the fracture walls — at constant normal spacing h — induce significant variations in the electrical and hydraulic conductance. These variations strongly depend on the orientation of the displacement $\vec{u}$. Their origin, and particularly their dependence on the radial geometry, will now be discussed theoretically.

5. Theoretical analysis of experimental data

In this section, spatial mean aperture fluctuations of a self-affine rough joint are first investigated with the help of numerical simulations. Then, the influence of the orientation of the displacement $\vec{u}$ on deviations from the parallel plane model found for the electrical and hydraulic conductances is discussed.

5.1. Numerical analysis of aperture fluctuations

Numerical simulations were previously used (Plourabouré et al., 1995) to analyze aperture variations with the relative displacement of rigidly translated self-affine surfaces kept in contact. Random two-dimensional self-affine surfaces are first generated numerically; they are defined by their height $z(x,y)$, and have the same statistical properties as the experimental fracture surfaces. A dichotomy algorithm introduced by Voss (1985) is used to generate self-affine surfaces with a roughness exponent close to the experimentally observed value ($\zeta = 0.8$), and with amplitudes similar to those of Table 1. Using normalization, such that the small-scale roughness amplitude remains constant, the standard deviation $\sigma_z(L)$ of the height of the surface increases with the sample size L following Eq. (6). The simulations reported here are purely geometrical (no fluid flow is computed); they analyze statistical fluctuations of the spatial mean aperture $h(u)$ from one realisation to another and, more specifically, deviations from the predictions of Eq. (3). The generated self-affine crack surfaces $z(x,y)$ are first translated by a vector $\vec{u}$, as displayed in Fig. 1. This allows the generation of the aperture field $a(x,y)$, and to determine numerically the normal relative displacement $h(\vec{u})$ for which the two translated surfaces are in contact. The procedure is repeated for a large number of realisations of the surface and of orientations of the displacement $\vec{u}$. The mean value $\langle h(u) \rangle$ and the standard deviation $\sigma_h(u)$ of the normal displacement h are finally computed.

Fig. 10 displays variations of these two parameters with u/L obtained from a large number of simulations in which the surface size increases from 128×128 to 1024×1024 points. These quantities increase with the relative displacement u/L, as observed

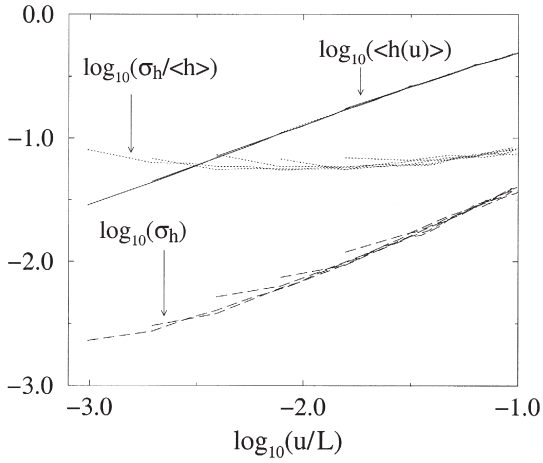

Fig. 10. Numerical simulations of the spatial mean aperture fluctuations. We plot in the log–log coordinates the variations of the mean aperture $\langle h \rangle$ averaged over 200 realisations (solid lines), the mean square deviation of the aperture σ_h (dashed lines), and the relative fluctuations of the aperture $\sigma_h / \langle h \rangle$ (dotted lines) vs. the relative displacement of the joint.

qualitatively in experiments. The ratio between $\sigma_h(u)$ and $\langle h(u)\rangle$, which represents the relative fluctuation of the aperture, has also been plotted and is roughly constant with u; this implies that both the aperture fluctuations and its mean value have the same dependence on the displacement (i.e. $\sigma_h \propto \langle h(u)\rangle$). This result is consistent with experimental geometrical measurements (Table 2), but the small number of available data points does not allow quantitative tests of the relation. Large fluctuations are also observed on the values of the electrical admittance in the same configuration of the surfaces for a given lateral displacement amplitude $|u|$ (Fig. 8a). As discussed above, a large fraction of these fluctuations is directly associated to the parameter σ_h through the linear relation between the normal displacement h and the electrical admittance A in the parallel plane model. The corresponding component σ_{Ah} of the fluctuations of the admittance will, thus, verify $\sigma_{Ah} \propto \sigma_h$ or $\sigma_{Ah} \propto \langle h(u)\rangle$. However, there still remains a significant scatter of the admittance for a fixed aperture once the admittance/aperture correlation has been taken into account, as can be seen in Fig. 8b. The corresponding fluctuation amplitude σ_{Af} also increases with u. In the following, the origin of such observed deviations from the parallel plane model is analyzed theoretically.

5.2. Deviations from parallel plane model

These deviations are studied here within the Reynolds approximation and in a radial flow geometry. Three possible origins of the fluctuations σ_{Af} will now be examined, namely, the influences of the finite sample size, of the local variability of the fracture aperture, and of a small angle of the fracture surface with respect to the horizontal plane.

•The first effect — purely geometrical — corresponds to the decrease of the length of the interval between the fracture walls from R to $R-u$ for a lateral translation $\vec{u}$. This effect would lead, from Eq. (7), to a systematic correction independent of the orientation of $\vec{u}$ for the value of the electrical admittance. This correction can be estimated through a first order Taylor expansion of Eq. (7), with respect to the parameter u/L, which leads to a term of order $|u|/(R\log(R/r_0))$. Numerical estimates of this correction using experimental parameters lead to a maximum deviation of 2.5% from linearity for the maximum relative displacement $u/L = 0.1$. This effect is one order of magnitude smaller than that observed in experiments, and can be neglected here for the electrical as well as for the hydraulic conductances.

•The local aperture variability may also modify the transport parameters. Previous analytical work (Dewitt, 1995) has analyzed the influence of permeability heterogeneities on the macroscopic permeability for parallel flows; the approach of this author is based on a perturbation expansion (Matheron, 1967) with respect to the relative amplitude of permeability fluctuations (assuming a weak disorder). The heterogeneous Darcy equation is expanded into a homogeneous one, assuming a small ratio between the standard deviation σ_k of the permeability and its mean value $\langle k\rangle$, i.e. $\sigma_k/\langle k\rangle < 1$ (the characteristic small parameter chosen is often the amplitude of log-permeability fluctuations; Matheron, 1967). This same approach can be applied to radial flows (Schwydler, 1963), and such expansions are also easily adapted to relative fluctuations of the aperture. The aperture field $a_u(x,y)$ can be written as a sum of the spatial mean

aperture $h(u)$ and of local fluctuations related to the height $z(x,y)$ of the individual surfaces

$$a_u(x,y) = \langle a_u(x,y)\rangle + \delta z = h(u) + z(x+u,y) - z(x,y). \tag{9}$$

The aperture field is assumed to be random but statistically homogeneous. The expected value of the aperture is independent of the point considered, and its standard mean deviation $\sigma(a_u)$ may be related to the translation u by $\sigma(a_u) = \sigma(\delta z) = Mu^{\zeta}$. Using Eq. (3), one sees that the expansion parameter $\sigma(a_u)/h(u)$ varies only slowly with u (logarithmic dependence). In the Reynolds approximation, by developing the effective conductance K_{el} with respect to the displacement u, one obtains $K_{\mathrm{el}} = h(u)(1 - \psi(u/L))$. The function $\psi(u/L)$ characterizes the deviation from the parallel plane model and varies only slowly with u: $\psi(u/L) = M/(K\sqrt{1 + K'\log(L/u)})$. This correction is much smaller than experimental deviations. Moreover, it depends only on the modulus $|\vec{u}|$ of the translation vector and not on its orientation, in contrast with the experimental results.

•A third possible origin of the deviation from the parallel plane model is a small angle of the plane of the joint with respect to the reference horizontal plane. Let us first estimate a simple correction in the case of a parallel flow. The electrical conductance is classically bounded by the harmonic and arithmetic spatial averages of the local conductance, which is proportional to the local aperture $a_u(x,y)$. In the limit of small fluctuations of $a_u(x,y)$ and small relative displacements $u/L \ll 1$, both upper and lower boundaries of the conductance have the same expression to first order

$$(1/S)\int\int a_u(x,y)\,\mathrm{d}x\,\mathrm{d}y\,h(u)\left(1 + \frac{u\phi}{h(u)}\right) \tag{10}$$

where S is the joint surface area, and ϕ is the average tilt angle of the surface with respect to the horizontal displacement plane. Eq. (10) predicts that the measured admittance will vary linearly with the tilt angle ϕ; quantitatively, for $\phi = 4°$, the estimated relative variation is of order 20%. Although actual tilt angles are somewhat smaller, the effect is strongly amplified by the radial flow geometry. In this case, the current increases close to the injection point as the inverse $(\sim 1/r)$ of the distance r. The effective slope ϕ in Eq. (10) then corresponds to a weighted average of local slopes with a particularly large influence of zones close to the injection point. Since the local slope in this region rarely coincides with the global plane of the fracture, ϕ may take values differing significantly from zero. In a more precise analysis, one must introduce the radius r_0 of the inner electrode as a new characteristic length scale. Two different types of behaviours are then expected, depending on the relative values of u and r_0.

(i) $u \ll r_0$ One recovers the previous effect due to the local tilt slope of the surface near the inner electrode, and the relative change of the conductance K_{el} compared to the case of parallel plates that K_{ref} obeys

$$\frac{K_{\mathrm{el}} - K_{\mathrm{ref}}}{K_{\mathrm{ref}}} = \frac{\log(R/r_0)}{2\pi h(u)}u\phi \tag{11}$$

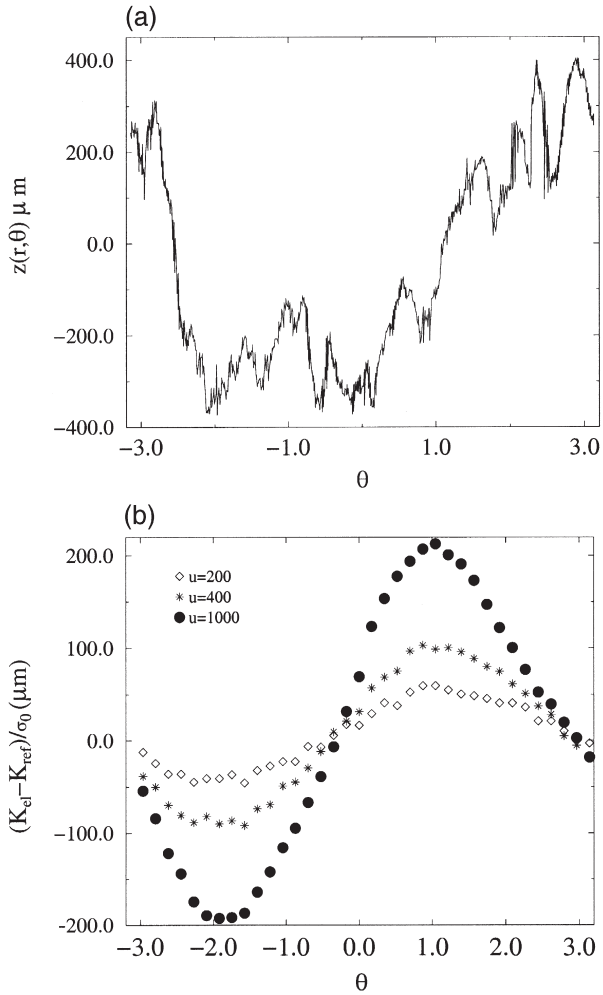

Fig. 11. (a) Height $z(r,\theta)$ of the surface along the boundary of the injection hole obtained from a mechanical profilometry. (b) Correction, $K_{\mathrm{el}} - K_{\mathrm{ref}}/\sigma_0$ (in μm), vs. the angle θ between $\vec{u}$ and reference axis, for different $u = \|\vec{u}\|$: ◇ $u = 200$ μm, * $u = 400$ μm, ● $u = 1000$ μm.

with

$$\phi = \left(\int z(r_0,\theta)\cos(\theta)\,\mathrm{d}\theta \right) / r_0 \tag{12}$$

in which the polar coordinates (r,θ) are centered at the injection point.

(ii) $u \gg r_0$ In this case, the edge effect near the electrode is negligible and the main contribution is due to a dipolar field

$$\frac{K_{\mathrm{el}} - K_{\mathrm{ref}}}{K_{\mathrm{ref}}} \propto \int \left(\frac{\vec{u}}{r^2} - \frac{2(\vec{u}\vec{r})\vec{r}}{r^4} \right) z(\vec{r})\,\mathrm{d}\vec{r}. \tag{13}$$

This integral is computed over the domain $r_0 < \|\vec{r}\| < R$. In order to estimate this effect, a two-dimensional height map of nearly 1 cm^2 close to the injection point has been analyzed using a mechanical profilometer to estimate the order of magnitude of expected corrections in the first regime (i) (the second regime (ii) would require a much larger map and will not be examined here). Fig. 11a shows the measured height $z(r_0)$ in a $r_0 = 3$ mm radius circle. Corrections due to the radial geometry were estimated both from a direct calculation on the two-dimensional map, and by computation of the tilt parameter ϕ from Eq. (12). These two methods give the same order of magnitude for the corrections.

Fig. 11b displays the correction deduced from a complete calculation of the radial geometry correction on conductances for different displacement amplitudes $u = \|\vec{u}\|$ and different angle θ between $\vec{u}$ and the reference axis Ox. This correction has to be compared to $2\pi h(u)/\log(R/r_0) \simeq 1.43 h(u)$, which can be estimated from Fig. 8a, and indicates that the mean plane tilt near the injection hole is responsible for an 18% deviation in conductance. This order of magnitude is in agreement with experimental measurements. A linear rescaling of the corrective term $(K_{el} - K_{ref})/u$ with u gives a satisfactory superposition supporting the linear dependence of the correction $K_{el} - K_{ref}$ indicated in the first regime (i) of Eq. (11). However, a rescaling $(K_{el} - K_{ref})/u^{\zeta}$ provides an equally good coincidence and supports the observation that $\Delta K/K$ is independent of u in regime (i).

To conclude, the deviation of the electrical conductance from the parallel plane behaviour observed in a radial geometry can be largely accounted for by a finite tilt angle of the fracture surface near the injection point. This result can be easily generalized to the hydraulic conductance, which leads to a relative correction term about three times larger than for the electrical conductance (the factor 3 results from the cubic law dependence of the hydraulic conductance on the aperture). Radial flow geometries are frequently encountered in configurations of practical interest, such as flow in fractures intersecting a borehole in oil reservoir or geothermal fields. The above analysis underlines the well-known fact that the structure of the rock near the borehole influences very much the flow properties in such geometries.

6. Conclusion

In the present paper, previous theoretical suggestions of scaling laws relating the electrical and hydraulic conductances of rough granite and basalt fracture joints, the relative normal and lateral displacements of the fracture surfaces, the total crack size, and the roughness exponent have been evaluated experimentally.

For purely geometrical aspects, finite-size effects on the relation between the lateral u and normal $h(u)$ displacements of complementary fracture surfaces have been confirmed with these self-affine surfaces kept in contact.

Concerning transport properties, it has first been observed that a simple parallel plane model gives a good first order approximation of the variation of electrical and hydraulic conductivities with the relative normal displacement h of crack surfaces. A more detailed analysis has confirmed that, as expected, the electrical conductance varies

linearly with the normal spacing h for complementary surfaces with no relative lateral displacement (this corresponds to a constant local distance between surfaces). On the contrary, when the two surfaces are displaced laterally, large relative deviations of few tens of percents from the linear dependence of the conductance on h are measured. These deviations increase with the lateral displacement and depend strongly on its direction. Such features are observed both for the hydraulic and the electrical conductances.

These observations have been analyzed in the frame of the Reynolds approximation using a first order perturbation theory. Our analysis shows that these fluctuations are associated with the radial flow geometry used in our experiments. The transport properties are strongly influenced by the geometry of the flow paths near the injection, and weakly perturbed by the flow field heterogeneity. In particular, we have shown that a small tilt angle between the global surface plane and the local orientation of the surface in the vicinity of the injection point may strongly influence the transport properties. Significant anisotropies of the conductance variations with respect to the direction of the relative displacement are also expected. Such a hypothesis can be verified by comparing the results obtained in the present work to experiments realised in a parallel flow geometry. In such configuration, deviation from the parallel plane approximation should be mainly due to the heterogeneity of the flow field, which will be well described by a first order weak disorder perturbation approximation.

Acknowledgements

We wish to gratefully acknowledge Y. Berthaud and J. Schmittbuhl for their help with the profilometry measurements, O. Pinet, J. Lacoste and S. Valette for their participation in the transport properties experiments, and O. Brouard and D. Vallet for the preparation of the experimental set-up. We also thank E.G. Flekkøy for the stimulating discussions and S. Tyler for his remarks and a careful reading of the manuscript. This work has been supported by the ECODEV ("ARC Géothermie des Roches Chaudes et Sèches"), PNRN and DBT programs, and by the GDR "Physique des Milieux Hétérogènes Complexes".

References

Bouchaud, J.P., Bouchaud, E., Lapasset, G., Planès, J., 1993. Models of fractal crack. Phys. Rev. Lett. 71 (14), 2240–2243.

Brown, S.R., 1985. Transport of fluid and electric current through a single fracture. J. Geophys. Res. 90, 5531.

Brown, S.R., 1986. Correlation between the surfaces of natural joint rocks. Geophys. Res. Lett. 13, 1430–1433.

Brown, S.R., 1987. Fluid flow through rock joints: the effect of surface roughness. J. Geophys. Res. 92 (B2), 1337–1348.

Brown, S.R., 1988. Correction to "A note on the description of surface roughness using fractal dimension". Geophys. Res. Lett. 15, 286.

Brown, S.R., 1995. Simple mathematical model of a rough fracture. J. Geophys. Res. [Solid Earth] 100 (B4), 5941–5952.

Brown, S.R., Chen, S., Sterling, J.D., 1989. Transport of fluid and electric current through a single fracture. J. Geophys. Res. 94, 9429–9438.
Dewitt, A., 1995. Effective permeability of heterogeneous porous media. Phys. Fluids 7 (11), 2553.
Evans, K.J., Kohl, T., Hopkirk, R.J., Rybach, L., 1992. Technical report, no. 359 to the Swiss National Energy Research Fund.
Falconer, K.J., 1990. Fractal Geometry: Mathematical Foundations and Applications. Wiley, New York.
Feder, J., 1988. Fractals. Plenum, New York.
Ge, S., 1997. A governing equation for fluid flow in rough fractures. Water Resour. Res. 33 (1), 53–61.
Gutfraind, R., Hansen, A., 1995. Study of hydrodynamic permeability of fractures using gas automata. Transp. Porous Media 18 (3), 131.
Matheron, G., 1967. Eléments Pour Une Théorie Des Milieux Poreux. Masson, Paris.
Mourzenko, V.V., Thovert, J.F., Adler, P.M., 1995. Validity of the Reynolds equation for flow through a single fracture. J. Phys. II (Paris) 5 (3), 465–482.
Mourzenko, V.V., Thovert, J.F., Adler, P.M., 1996. Geometry of simulated fractures. Phys. Rev. E 53 (6), 5006–5026.
Petitjean, L., Couet, B., 1994. Modelling of fracture propagation during overbalanced perforating. Technical Report ISD0029401a, Ridgefield Schlumberger–Doll research center, US.
Pinkus, O., Sternlicht, B., 1961. Theory of Hydrodynamical Lubrication. McGraw-Hill, New York.
Plouraboué, F., Kurowski, P., Hulin, J.P., Roux, S., Schmittbuhl, J., 1995. Aperture of rough cracks. Phys. Rev. E 51 (3), 1675.
Plouraboué, F., Winkler, K., Petitjean, L., Hulin, J.P., Roux, S., 1996. Experimental study of the influence of crack velocity on fracture surface roughness of rocks. Phys. Rev. E 53 (1), 5684.
Poon, C.Y., Sayles, R.S., Jones, T.A., 1992. Surface measurement and fractal characterisation of naturally fractured rocks. J. Phys. D: Appl. Phys. 25, 1269–1275.
Power, W.L., Tullis, T.E., Brown, S.R., Boitnott, G., Scholz, C.H., 1987. Roughness of natural fault surface. J. Geophys. Res. 14, 29–32.
Rasmuson, A., Neretnieks, I.J., 1982. Chemical transport in a fissure rock: verification of a numerical model. Water Resour. Res. 18 (5), 1479–1492.
Roux, S., Schmittbuhl, J., Vilotte, J.P., Hansen, A., 1993. Some physical properties of self-affine rough surfaces. Europhys. Lett. 23 (4), 277–282.
Schmittbuhl, J., Berthaud, Y., Roux, S., 1995. Development of roughness in crack propagation. Europhys. Lett. 28 (8), 585–590.
Scholz, C., 1990. The Mechanics of Earthquakes and Faulting. Cambridge Univ. Press, New York.
Schwydler, M., 1963. Sur la precision du debit des puits. Izv. Akad. Nauk SSSR, Mekh. Mashinostr. 5 (5), 148–150.
Tsang, Y.W., Tsang, C.F., Neretnieks, I., Moreno, L., 1988. Flow and tracer transport in fractures media: a variable aperture channel model and his properties. Water Resour. Res. 24 (12), 2049–2060.
Voss, R.F., 1985. In: Earnshaw, R.A. (Ed.), Fundamental Algorithms in Computer Graphics. Springer-Verlag, Berlin, pp. 805–835.
Witherspoon, P.A., Wang, J., Iwai, K., Gale, J.E., 1980. Validity of cubic law for fluid flow in a deformable rock fracture. Water Resour. Res. 16, 1016–1024.
Zimmerman, R., Kumar, S., Bodvarsson, G., 1991. Lubrification theory analysis of the permeability of rough-walled fractures. Int. J. Rock Mech. Min. Sci. 28 (4), 324–331.